Eur. Phys. J. D (2018) 72: 227
https://doi.org/10.1140/epjd/e2018-90333-2

THE EUROPEAN PHYSICAL JOURNAL D

Regular Article

Electron capture, excitation and ionization processes in He^{2+}–H collisions in dense quantum plasmas

Dragan Jakimovski[1,a] and Ratko K. Janev[2]

[1] Department of Physics, Sts Cyril and Methodius University, PO Box 162, 1000 Skopje, Macedonia
[2] Macedonian Academy of Sciences and Arts, PO Box 428, 1000 Skopje, Macedonia

Received 7 July 2018 / Received in final form 4 October 2018
Published online 21 December 2018

Abstract. Electron capture, excitation and ionization processes in He^{2+}–H collisions taking place in quantum plasmas are studied by employing the two-center atomic orbital close coupling (TC-AOCC) method. The Debye-Hückel-cosine (DHC) potential is used to describe the plasma screening effects on the Coulomb interaction between charged particles. The properties of eigenenergies of hydrogen-like atom with DHC potential are investigated as function of the screening length of the potential. It is found that the binding energies of nl states decrease with decreasing the screening length of the potential. The dynamics of excitation, electron capture and ionization processes in He^{2+}–H collision system is investigated when the screening length of the potential varies for a wide collision energy range. The TC-AOCC cross sections are compared with those for the pure Coulomb potential and, for the total electron capture, with the results of classical trajectory Monte Carlo method.

1 Introduction

The plasma screening effects on the atomic structure and radiative and collision processes taking place in a plasma environment have been subject to extensive studies in last several decades. Most of these studies have been performed for the weakly coupled classical plasmas in which the interaction between charged plasma particles is described by the well-known Debye-Hückel potential $V(r) = -Ze^2 \exp(-r/\lambda)/r$ [1], where Ze is the positive ion charge, e is the elementary charge and $\lambda = (k_{\rm B}T_e/4\pi n_e^3)^{1/2}$ is the Debye length with $T_e, n_e, k_{\rm B}$ being the electron plasma temperature, density and the Boltzmann constant. The validity of Debye-Hückel potential for describing the screened interaction in a weakly coupled classical plasma requires the condition $\lambda \geq \bar{a} = (3/4\pi n_e)^{1/3}$, where $\bar{a}$ is the average interparticle distance.

Many theoretical studies of electronic structure and radiative properties of one-electron atomic systems and their electron, photon and ion-impact collision processes have been performed in weakly coupled plasmas using Debye-Hückel potential and reviewed recently [2]. In plasmas with temperatures lower than the electron Fermi temperature $T_{\rm F}(= \hbar^2(3\pi^2)^{2/3}n^{2/3}/2m)$ ($\hbar$ being the reduced Planck constant) and densities such that de Broglie wavelength $\lambda_{\rm B}(= \hbar/mv_{th})$ (v_{th} is the thermal velocity, m is the electron mass) satisfies the condition $\lambda_{\rm B} \geq \bar{a}$, the quantum effects (quantum tunneling, quantum diffraction, etc.) start to become important (quantum plasmas). Quantum plasmas are observed in metals, nanoscale structures, semiconductor devices and in compact astrophysical objects (e.g. neutron stars, white dwarfs). The interaction between a positive charge Ze and an electron in such plasmas has the form [3]

$$V(r) = -\frac{\mathrm{Ze}^2}{r} \exp\left(-\frac{r}{\kappa}\right) \cos\left(\frac{r}{\kappa}\right) \tag{1}$$

where $\kappa = 2^{1/2}/k_q$ and $k_q = \left(4m^2\omega_p^2/\hbar^2\right)^{1/4}$ is the electron quantum wavenumber and $\omega_p = \left(4\pi e^2 n_e/m\right)^{1/2}$ is the plasma frequency. We note that for infinitely large screening lengths κ the potential (1) reduces to the pure Coulomb potential. It should also be noted that the screening length κ does not depend on the plasma temperature, implying that the quantum plasmas are both strongly coupled ($\Gamma = e/\bar{a}k_{\rm B}T_e \gg 1$) and degenerate ($\Theta = k_B T_e/T_F \ll 1$). The screening potential (1) also does not account for the quantum electron-exchange correlation effects, nor does it include the finite-temperature gradient-correction effects to the kinetic energy. The account of these effects leads to a more complex screening potential [4] with two mutually related screening lengths, but the calculations performed with this potential in [5] for the electron capture to $1s, 2l$ and $3l$ states in $H^+ + H$ collisions [6] for $T_e = 0.09\,\mathrm{eV}$ and $n_e = 8.19 \times 10^{18}\,\mathrm{cm}^{-3}$ in the energy range 5–200 keV show very good agreement with the results obtained in reference [6] with the potential (1) for the same plasma parameters. The conditions

[a] e-mail: dragan.jakimovski@gmail.com

$\Gamma \gg 1$ and $\Theta \ll 1$ are satisfied in all solid state plasmas ($n_e \sim 10^{22}$–$10^{24}\,\mathrm{cm}^{-3}$, $T_e \leq 0.1\,\mathrm{eV}$), white dwarf plasmas ($n_e \sim 10^{26}$–$10^{29}\,\mathrm{cm}^{-3}$, $T_e = 0.1$–$100\,\mathrm{eV}$) and in some parametric regions of ultra-short-pulse laser produced ($n_e \sim 10^{21}$–$10^{24}\,\mathrm{cm}^{-3}$, $T_e = 0.1$–$100\,\mathrm{eV}$) and inertial confinement fusion ($n_e \sim 10^{22}$–$10^{26}\,\mathrm{cm}^{-3}$, $T_e = 50$–$300\,\mathrm{eV}$) plasmas.

Atomic structure properties and collision processes in quantum plasmas involving the potential (1) have received a considerable attention in recent years [6–17]. In particular, the electron capture process in $H^+ + H$ collisions has been studied in references [6,14] by employing the CTMC and TC-AOCC methods, respectively. The CTMC method with this potential was also used to study the electron capture in $He^{2+} + H$ collisions [15]. In the present work, we shall study the dynamics of excitation, electron capture and ionization processes in $He^{2+} + H$ collisions taking place in a quantum plasma

$$He^{2+} + H(1s) \rightarrow He^{2+} + H(nl) \quad (2a)$$
$$\rightarrow He^{+}(nl) + H^{+} \quad (2b)$$
$$\rightarrow He^{2+} + H^{+} + e \quad (2c)$$

by employing the TC-AOCC method with a large expansion basis. We shall examine the structural properties of the hydrogen atom with the potential (1), the dependence of partial (state-selective) cross sections of reactions (2a) and (2b) on the screening length κ and compare them with the results of unscreened Coulomb interaction and, in the case of reaction (2b), with the available total electron capture CTMC result of reference [15].

The motivation for undertaking this study is to investigate the dynamics of processes of type (2) in a heteronuclear collision system and compare it with the one in the homonuclear $H^+ + H(1s)$ system, considered in reference [6]. It is well-known that, due to the difference in nuclear symmetry, the multistate coupling dynamics in these two collision systems in the case of unscreened Coulomb interactions is quite different, especially at low collision energies [18]. It is, therefore, of interest to investigate these differences in the case of a screened potential, as well as the effect of increased projectile charge. This investigation will be done on the level of transition matrix elements and cross sections for a given screening lenghts, including the ionization process (2c), not considered in [6].

The organization of the article is as follows. In Section 2, we discuss the properties of eigenenergies of hydrogen-like atoms with the interaction (1). In Section 3, we shall outline the TC-AOCC computational method used for description of the collision dynamics of reactions (2) and in Section 4 we present and discuss our results. Finally, in Section 5 we give our conclusions.

In the remainder of this paper we shall use atomic units, unless otherwise explicitly indicated.

2 Properties of eigenenergies of hydrogen atom with the DHC potential (1)

The most important properties of DHC potential (1), that decreases faster than $-1/r^2$ when $r \rightarrow \infty$, are the lifting of degeneracy of angular momentum states and the finite number of bound states supported by the potential for any finite value of the screening length [19]. The latter property implies that the energies E_{nl} of bound states decrease with decreasing length κ. At certain critical value κ^c_{nl} the binding energy of nl state becomes zero and the state enters the continuum (and remains there for all $\kappa \leq \kappa^c_{nl}$). It should be noted that the radial Schrödinger equation with the potential (1) is scalable with respect to the charge Z [6], so that the energies of a hydrogen-like ion are scaled as $\varepsilon_{nl} = E_{nl}/Z^2$ and screening lengths as $\delta = Z\kappa$. The scaled energies of the nl ($n \leq 3$) states of a hydrogen-like atom with the potential (1) as function of the scaled screening length δ, calculated by the method described in Section 3, are shown in Figure 1. In Table 1, we give the scaled critical screening lengths δ^c_{nl} for the states with $n \leq 6$. The table shows that for a given value of δ only a finite number of states remain bound in the potential and that the critical screening length increases with increasing the angular momentum quantum number l for a given value of the principal quantum number n. It should be remarked that relation $\delta = Z\kappa$ implies that for any given value of κ_0 in the region $\kappa < \kappa_0$ there will be twice more bound states in He^+ than in H as illustrated in Table 1. This fact introduces significant differences in the dynamics of $He^{2+} + H$ and $H^+ + H$ collision systems.

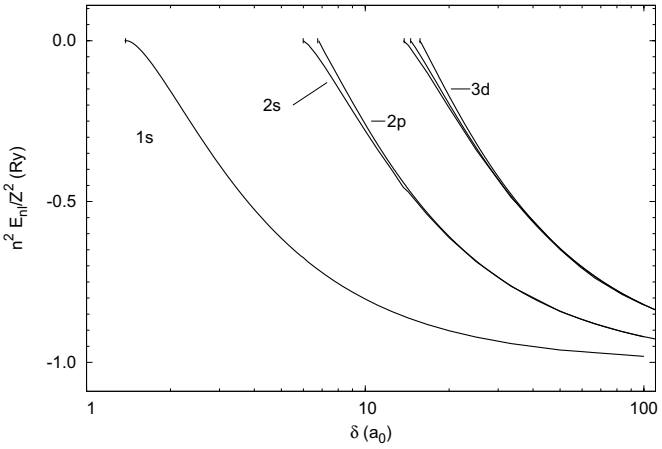

Fig. 1. Scaled energies of $1s$, $2l$ and $3l$ states of hydrogen-like atom in the potential (1) as function of scaled screening length $\delta = Z\kappa$.

3 Computational method

For calculation of the cross sections of reactions (2) we shall employ the TC-AOCC method, described in detail elsewhere [18,20]. The total scattering wave function in this method is expanded in terms of electronic states centered on both centers. For determining the bound electronic states with the potential (1) on either of the two centers, one uses the variational method with even-tempered trial functions [21]

$$\chi_{klm}(\mathbf{r};\delta) = N_l(\xi_k(\delta))\, r^l e^{-\xi_k(\delta) r} Y_{lm}(\hat{\mathbf{r}})$$
$$\xi_k(\delta) = \alpha\beta^k, \quad k = 1, 2, \ldots, N \quad (3)$$

Table 1. Scaled critical screening lengths δ_{nl}^c (in a_0) for $n \leq 6$ states in the potential (1).

n/l	0	1	2	3	4	5
1	1.3858					
2	5.9974	6.7474				
3	13.7982	14.5534	15.7278			
4	24.7260	25.4687	26.7343	28.3758		
5	38.7660	39.5007	40.8161	42.5855	44.6999	
6	55.9179	56.6496	57.9944	59.8509	62.1138	64.7020

where $N_l(\xi_k)$ is a normalization constant, $Y_{lm}(\hat{\mathbf{r}})$ are the spherical harmonics and α and β are variational parameters, determined by minimization of the energy for each value of the screening length δ. The atomic states $\phi_{nlm}(\mathbf{r};\delta)$ are then obtained as linear combinations

$$\phi_{nlm}(\mathbf{r};\delta) = \sum_k c_{nk}(\lambda)\chi_{klm}(\mathbf{r};\delta) \tag{4}$$

where the coefficients c_{nk} are determined by diagonalization of single-center Hamiltonian. This diagonalization yields the energies $\varepsilon_{nl}(\delta)$ of the bound states in the DHC potential (1). In order to describe the ionization process, one needs to include in the expansion basis (4) also states with positive energies (pseudostates) centered on either of the centers. It is natural to place them on the target, since the dominant part of ejected electron distribution is expected to be around the target.

The total electron wave function Ψ is expanded in terms of atomic orbitals (4) centered on the target (T) and projectile (P) (each orbital multiplied by a plane wave electron translational factor to satisfy the boundary conditions) [18,20]

$$\Psi(\mathbf{r},t;\kappa) = \sum_i a_i(t)\phi_i^T(\mathbf{r},t;\kappa) + \sum_j b_j(t)\phi_j^P(\mathbf{r},t;2\kappa) \tag{5}$$

in which the basis $[\phi_i^T(\mathbf{r},t;\kappa)]$ includes also the wave functions of continuum pseudostates (we denote them by $\tilde{\phi}_i^T(\mathbf{r},t;\kappa)$ and their amplitudes by $\tilde{a}_i(t)$. In the second term of equation (5) the argument of the traveling orbital contains the screening length $\delta = Z\kappa = 2\kappa$ because the projectile has charge $Z = 2$. While, as mentioned earlier, the wave functions and energies of one-electron systems **H** and $\mathbf{He}^+$ can be scaled, in the collision problem involving the different target and projectile potentials (see below) they have to be used in unscaled form.

By inserting equation (5) in the time dependent Schrödinger equation $i\partial\Psi/\partial t = H\Psi$, where $H = -\nabla_r^2/2 + V^T(r_T) + V^P(r_P)$ and $V^{T,P}(r_{T,P})$ have the form of equation (1), one obtains the coupled equations for the amplitudes $a_i(t)$ and $b_j(t)$ [18,20]

$$i(\dot{\mathbf{A}} + \mathbf{S}\dot{\mathbf{B}}) = \mathbf{H}\mathbf{A} + \mathbf{K}\mathbf{B} \tag{6a}$$

$$i(\dot{\mathbf{B}} + \mathbf{S}^\dagger\dot{\mathbf{A}}) = \bar{\mathbf{K}}\mathbf{A} + \bar{\mathbf{H}}\mathbf{B} \tag{6b}$$

where **A** and **B** are the vectors of the amplitudes $a_i(t)$ and $b_j(t)$, respectively. **S** is the overlap matrix ($\mathbf{S}^\dagger$ is its transposed form), **H** and $\bar{\mathbf{H}}$ are direct coupling matrices involving the states on the target and projectile, respectively, and **K** and $\bar{\mathbf{K}}$ are the i–j and j–i electron exchange matrices. The solutions of the system of equations (6), under the initial conditions $a_i(-\infty) = \delta_{1i}$, $b_i(-\infty) = 0$, with a rectilinear trajectory for the nuclear motion, yield for the $1 \to i$ excitation and $1 \to j$ charge exchange cross sections the following expressions

$$\sigma_{ex,j} = 2\pi \int_0^\infty |a_j(\infty)|^2 b\mathrm{d}b \tag{7a}$$

$$\sigma_{cx,j} = 2\pi \int_0^\infty |b_j(\infty)|^2 b\mathrm{d}b \tag{7b}$$

where b is the impact parameter. The ionization cross section is given by

$$\sigma_{ion} = \sum_i 2\pi \int_0^\infty |\tilde{a}_i(\infty)|^2 b\mathrm{d}b \tag{7c}$$

where $\tilde{a}_i(t)$ are the amplitudes of continuum pseudostates.

In solving the coupled equation (6) we have used an expansion basis containing all bound states on He^+ with principal quantum number $n \leq 5$ (in total 35 states), and on the target we have used all bound states with $n \leq 6$ plus the $7s$ bound state. In addition, in the basis centered on H we have included 117 positive energy pseudostates, making the total of 174 states centered on H. This basis was also used in the calculations of excitation, electron capture and ionization processes in $He^{2+} + H$ collisions in the plasma free (pure Coulomb interaction) case in reference [22], where it was demonstrated that it provides convergent results. By comparing the results of present calculations for different screening lengths with those of reference [22] we can see the plasma screening effects of the Coulomb interaction on the cross sections of considered processes.

As mentioned earlier, in order to demonstrate the difference between the cross sections of reactions (2) in the $He^{2+} + H(1s)$ and $H^+ + H(1s)$ systems with the potential (1), we have performed calculations also for $H^+ + H$ for the screening length $\kappa = 10a_0$. When calculating the cross sections in the $H^+ + H(1s)$ system we have used the same basis sets as for $He^{2+} + H$.

An insight in the difference of collision dynamics in these two systems can be gained already on the level of matrix elements for specific transitions in processes (2) and for a given screening length. In Figures 2a–2c we present respectively the matrix elements as function of

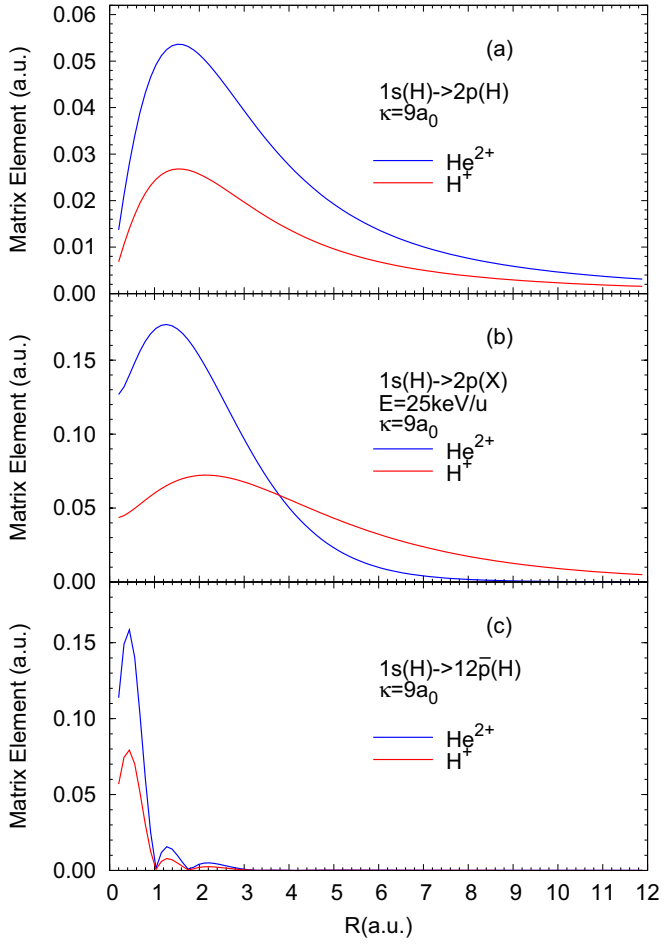

Fig. 2. Matrix elements for the excitation (a), electron capture (b) $1s \to 2p$ transitions and for the ionizing transition to the $12\bar{p}$ continuum pseudostate (c).

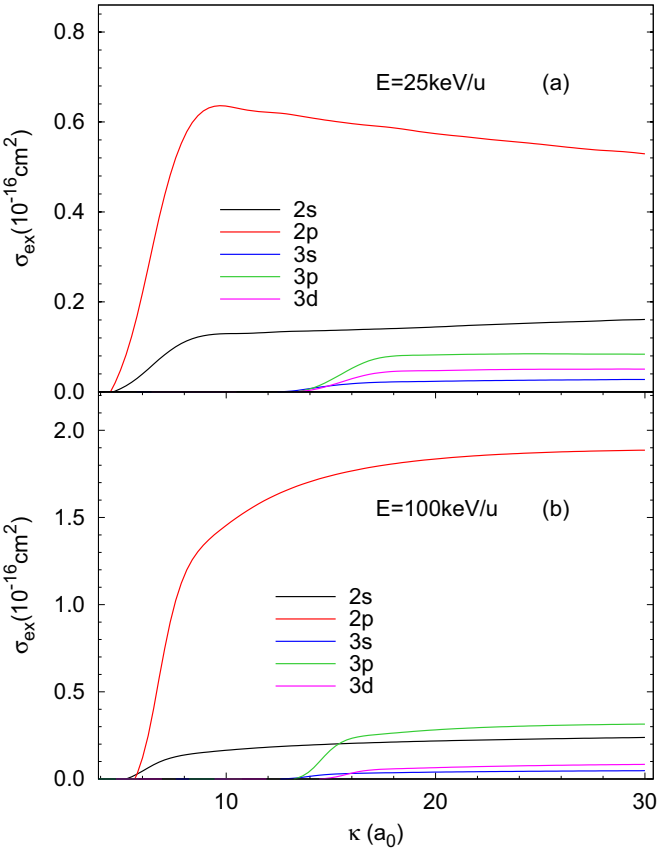

Fig. 3. Dependence of the $2l$ and $3l$ excitation cross sections on the screening length κ for the collision energies of 25 keV/u (a) and 100 keV/u (b).

internuclear distance R for the excitation $1s \to 2p$, electron capture $1s \to 2p$ (at $E = 25\,\mathrm{keV/u}$) and ionizing $1s \to 12\bar{p}$ transitions for a screening length $\kappa = 9a_0$, where $12\bar{p}$ is a continuum pseudostate, arising from entering in the continuum of the $12p$ Coulomb state when the potential is screened. The two zero minima at small R in the matrix element for transition to the $12\bar{p}$ continuum pseudostate are due to the nodes of this function. The amplitude of $12\bar{p}$ wave function decreases rapidly with increasing the radial distance and the effects of its distant eight nodes are not visible in Figure 2c. The larger values of excitation and ionizing matrix elements for the $He^{2+} + H$ system for all R is obviously a reflection of the stronger electron-projectile interaction than in the $H^+ + H$ case. In the case of electron capture matrix element the effect of larger projectile change is manifested in squeezing the radial distribution of $2p$ electron capture state towards the smaller distances, thus making its values at large R smaller than those for the $H^+ + H$ case.

However, the main difference in the collision dynamics in the $He^{2+} + H(1s)$ and $H^+ + H(1s)$ systems results form the different number of the bound n, l states on the projectile for a given screening strength of the potential. From the Z-scaling of radial Schrödinger equation with the potential (1) it follows that for a given κ there will be twice more bound n, l states on He^+ than on H, enshrined also in the relation $\delta = Z\kappa$ (see Tab. 1).

4 Results and discussion

4.1 Excitation

We first consider the dependence of cross sections for excitation to $2l$ and $3l$ states of H on the screening length κ for two typical collision energies of 25 keV/u and 100 keV/u. (We note that for the H spectrum, $\kappa = \delta$.) The results are shown in Figures 3a and 3b, respectively. It is observed that for both energies the cross section for excitation to the $2p$ state is considerably larger than for the other states for all values of the screening length, resulting from the dipole character of $1s \to 2p$ transition. It should be remarked, however, that the $2p$ cross section for $E = 25\,\mathrm{keV/u}$ exhibits a maximum at $\kappa \approx 9a_0$, after which it slowly decreases with increasing κ towards its limiting value at $\kappa = \infty$ (plasma free case). In contrast, the $2p$ excitation cross section for $E = 100\,\mathrm{keV/u}$, after its sharp increase at κ slightly above the critical screening length κ^c_{2p}, slowly increases with increasing κ. The $2s$ excitation cross section for both energies shows a mild increase with

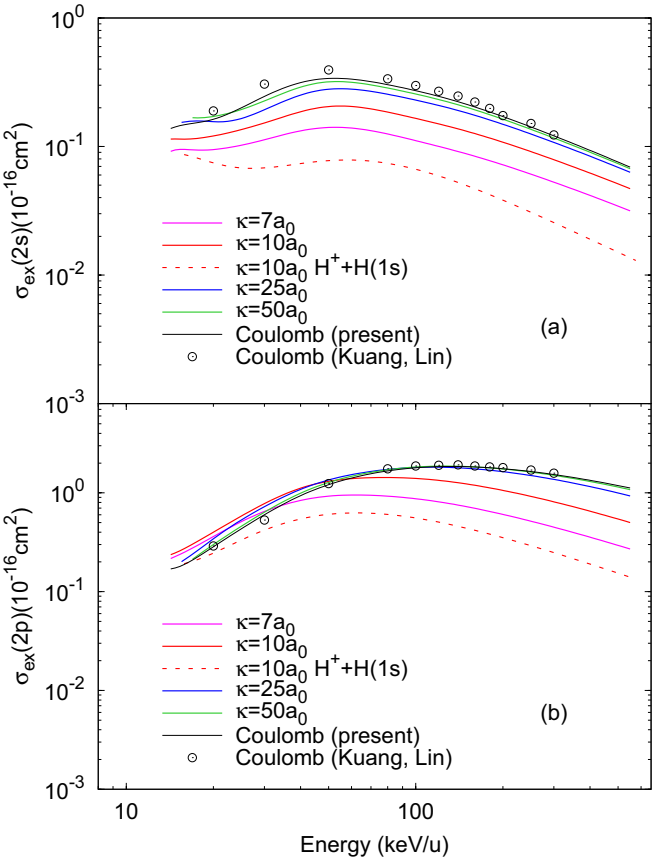

Fig. 4. Energy dependence of $2s$ (a) and 2p (b) excitation cross sections for $\kappa = 7$, 10, 25, $50a_0$ compared with the plasma free cross sections of present calculations (Coulomb) and those of reference [22] (Kuang and Lin; symbols). The dashed lines for $\kappa = 10a_0$ refer to $H^+ + H$ collision system.

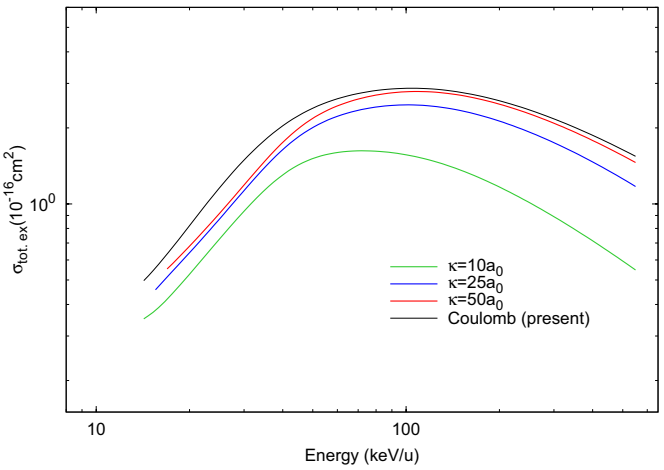

Fig. 5. The total excitation cross section for a plasma with $\kappa = 10$, 25, $50a_0$ and for the unscreened Coulomb interaction.

increasing κ. All $3l$ excitation cross sections, after leaving the neighborhood of the critical screening lengths κ^c_{3l}, quickly reach a plateau.

In Figure 4 we show the energy dependence of the $2s$ (Fig. 4a) and $2p$ (Fig. 4b) excitation cross sections for the screening lengths $\kappa = 7$, 10, 25 and $50a_0$ in the interval ∼15–600 keV/u, together with the results for the unscreened Coulomb potential performed in the present work and the results of Kuang and Lin [22]. It can be observed in the figures that the energy dependences of $2s$ and $2p$ excitation cross sections for different values of κ are somewhat different. The $2s$ cross section for a given value of κ is always smaller than the pure Coulomb cross section in the energy region above ∼20 keV/u, it increases with increasing κ and for $\kappa = 50a_0$ it approaches the cross section with pure Coulomb interaction. In contrast, the $2p$ cross section in the region below ∼40 keV/u increases with decreasing κ, but above this energy it decreases with decreasing κ. This behavior of $2s$ and $2p$ excitation cross sections is consistent with their κ-dependences in Figure 3. The physical origin of this difference lies in the difference of the radial electron distributions of $2s$ (more compact) and $2p$ (more diffused) states. At high collision energies the excitation process involves the inner parts of these distributions whose dependence on κ is similar (both decrease with increasing κ), while at low collision energies the asymptotic parts of these distributions for which the more diffused $2p$ distribution shows a much faster increase with decreasing κ than that for $2s$ (see [6]).

Figure 4 shows that the $2s$ and $2p$ excitation cross sections, calculated in the present work for the pure Coulomb case (full black lines) coincide with the plasma-free results of Kuang and Lin [22] (symbols). In Figure 4, we also show the $2s$ and $2p$ excitation cross sections for the $H^+ + H$ collision system for the screening length $\kappa = 10a_0$. With respect to the cross sections in the $He^{2+} + H$ system the proton impact $2s$ and $2p$ cross sections for this screening length are significantly smaller in the considered energy range. The difference increases with increasing the collision energy and at $E = 600$ keV/u, the cross sections for $He^{2+} + H$ are about four times larger than those for $H^+ + H$, consistent with the Z^2 high-energy Born scaling of excitation cross sections.

We have calculated also the cross sections for excitation to $3l$, $4l$ and $5l$ states $\kappa = 10$, 25, $50a_0$. Their values are increasingly smaller than those for the $2l$ states. The summed (very close to the total) cross section is shown in Figure 5, together with that for the pure Coulomb interaction. The general increase of the excitation cross section with increasing the screening length is due to the fact that for large values of κ increasingly more states remain bound in the potential that can participate in the excitation dynamics.

4.2 Electron capture

In Figure 6 we show the κ dependence of $2l$ and $3l$ electron capture cross sections for $E = 25$ keV/u (Fig. 6a) and $E = 100$ keV/u (Fig. 6b). The capture states $2l$ and $3l$ belong to the He^+ ($Z = 2$) spectrum and the critical screening lengths κ^c_{nl} are now twice smaller than those for the H spectrum, $\kappa^c_{nl} = \delta^c_{nl}/2$ (compare with Fig. 3). The capture to $1s$ state is not included in the panels since its values are negligibly small at all energies due to the large difference between the $He^+(1s)$ and $H(1s)$ energy levels. On the other hand, the $H(2l)$ energy levels are

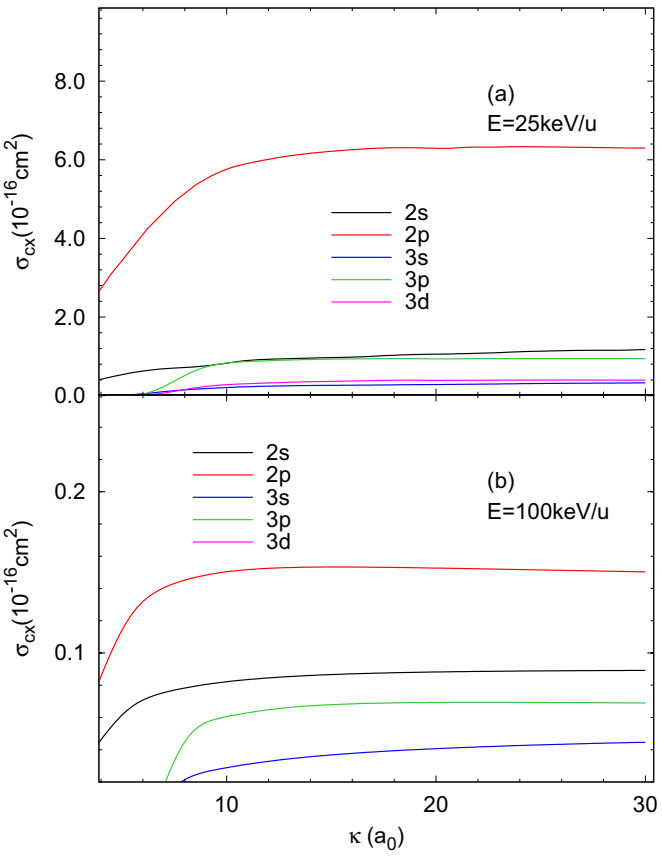

Fig. 6. Dependence on the scaled screening length κ of electron capture cross sections to $2l$ and $3l$ projectile states at $E = 25\,\mathrm{keV/u}$ (a) and $E = 100\,\mathrm{keV/u}$ (b).

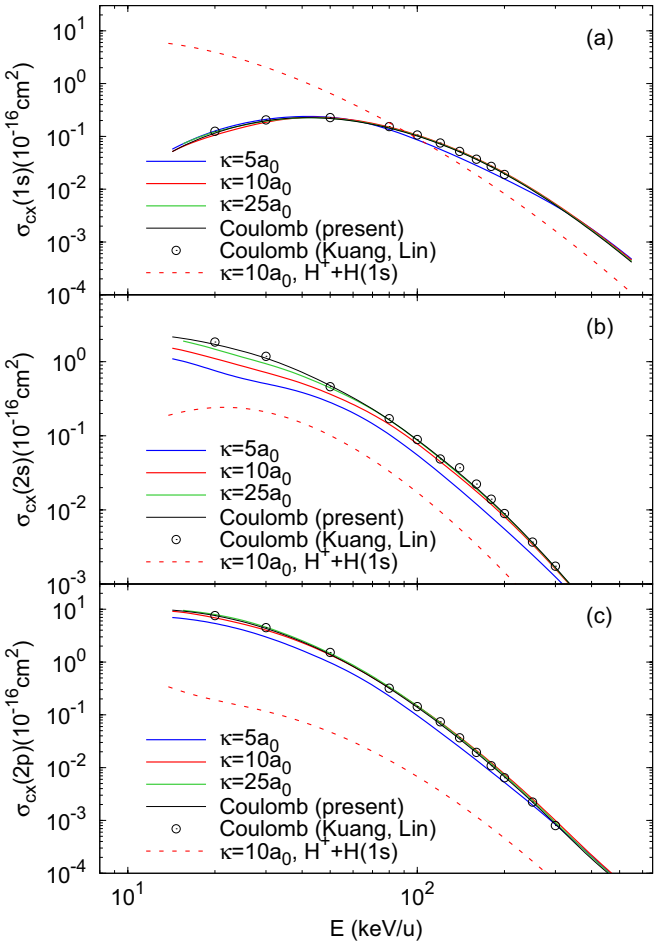

Fig. 7. Energy dependence of cross sections for electron capture to $2s$ (a) and $2p$ (b) projectile states for $\kappa = 5$, 10, $25a_0$ and for the pure Coulomb interaction. The symbols are the results of reference [22] for the pure Coulomb interaction case. The dashed lines are the cross sections for the $H^+ + H$ collision for the screening length $\kappa = 10a_0$.

close to the energy of $He^+(1s)$ state for all κ when the $H(2l)$ and $He^+(1s)$ are bound. Figure 6 shows that, like in the case of excitation, for both selected energies the cross section for capture to $2p$ state of the projectile is larger than for other transitions. This is a result of the large direct dipole $1s \to 2p$ coupling of the initial and final states. In all other cases, the population of the final state involves multiple interstate transitions. After the threshold κ^c_{nl} the cross section slowly, for $E = 25\,\mathrm{keV/u}$, and much faster, for $E = 100\,\mathrm{keV/u}$, increases with increasing κ and reaches a region of saturation or very slow increase (for $2s$, $3s$ and $3p$ for $E = 100\,\mathrm{keV/u}$). The mild undulations on the $2p$ cross section for $E = 25\,\mathrm{keV/u}$ are effects of the κ^c_{nl} thresholds of upper states at which they become coupled with the $2p$ state. For the higher energy $E = 100\,\mathrm{keV/u}$ these effects are smeared out as the collision time is small.

The energy dependence of dominant electron capture channels to $1s$, $2s$ and $2p$ projectile states is shown respectively in Figures 7a, 7b and 7c, in the energy range ~15–500 keV/u. Quantum plasmas with screening lengths $\kappa = 5$, 10, $25a_0$ are selected. The cross sections for capture to these states in the plasma-free case are also shown, including the results of Kuang and Lin [22]. Included in this figure are also the $1s, 2s$ and $2p$ capture cross sections in the $H^+ + H$ collisions for the screening case with $\kappa = 10a_0$. It should be noted that, the initial $H(1s)$ is quasi-isoenergetic with the $He^+(2s)$ and $He^+(2p)$ states for $\kappa \geq 4a_0$, ($\delta \geq 8a_0$) but very different from the energy of $He^+(1s)$ (see Fig. 1). In the $H^+ + H$ system the initial and final $H(1s)$ states are isoenergetic for all κ, while the energy difference between the initial and $2s, 2p$ capture states is large. These relations between the energies of initial $1s$ and final $2s, 2p$ states in the $He^{2+} + H$ and $H^+ + H$ collision systems make the reactions for electron capture to $He^+(2s \text{ or } 2p)$ and $H(1s)$ quasi-resonant and resonant, respectively, and highly non-resonat for capture to $He^+(1s)$ and $H(2s \text{ or } 2p)$. These reaction properties are clearly manifested in the energy behavior and magnitues of electron capture cross sections in Figure 7. The $2s$ and $2p$ cross sections for capture to He^{2+} projectile show an energy behavior typical for a resonant electron capture reaction (steady increase with decreasing the energy), whereas the one for capture to the $1s$ state shows a typical behavior for a non-resonant electron capture reaction (a broad maximum around ~5 keV/u). At the same time,

for energies below ∼150 keV/u, where the reaction energy defect plays the dominant role in the reaction dynamics, the resonant $2s$ and $2p$ cross sections are significantly larger than the $1s$ cross section (above this energy the momentum transfer becomes the dominant reaction mechanism [18], and the capture to a tightly bound state is preferred). In the $H^+ + H$ collision, the energy behavior and magnitudes of the cross sections for capture to $1s, 2s$ and $2p$ for plasma screening with $\kappa = 10a_0$ have just the opposite properties. The observed larger values of the non-resonant cross section for capture to $He^+(1s)$ for screening $\kappa = 10a_0$ relative to the resonant cross section for capture to $H(1s)$ with the same plasma screening for energies above ∼80 keV/u (cf. Fig. 7a) result from the larger nuclear charge of the projectile. This charge effect is also present in the $2s$ and $2p$ cross sections at high energies.

In Figure 7 we observe that with increasing the screening length κ the $1s, 2s$ and $2p$ capture cross sections rapidly increase towards the cross section for the pure Coulomb interaction, with which they coincide already for $\kappa = 25a_0$. This cross section increase with κ is much faster than in the case of excitation cross sections in Figure 4 and is a consequence of the larger number of coupled bound states on He^+ than on H for a given value of κ.

We have performed cross section calculations also for capture to $3l$, $4l$ and $5l$ states for $\kappa = 4.44a_0$ and $\kappa = 10a_0$ and for the pure Coulomb interaction. For these two screening lengths classical-trajectory Monte Carlo (CTMC) calculations with the potential (1) have been performed in reference [15]. Our summed (total) cross sections for these two screening lengths are shown in Figure 8, together with the results of reference [15]. The comparison of CTMC and present TC-AOCC results for the two screened potential cases shows that, except for energies below ∼30–35 keV/u, the CTMC results are larger than the TC-AOCC results. The present result for the pure Coulomb interaction case coincides with the result of reference [22].

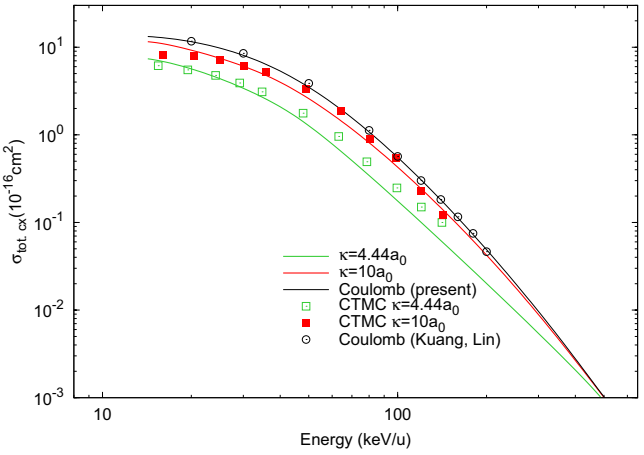

Fig. 8. Total electron capture cross sections for plasmas with screening lengths $\kappa = 4.44a_0$ and $\kappa = 10a_0$ and for the plasma-free case. Present results: full lines; symbols: results from reference [15] (screened interaction) and reference [22] (unscreened Coulomb interaction).

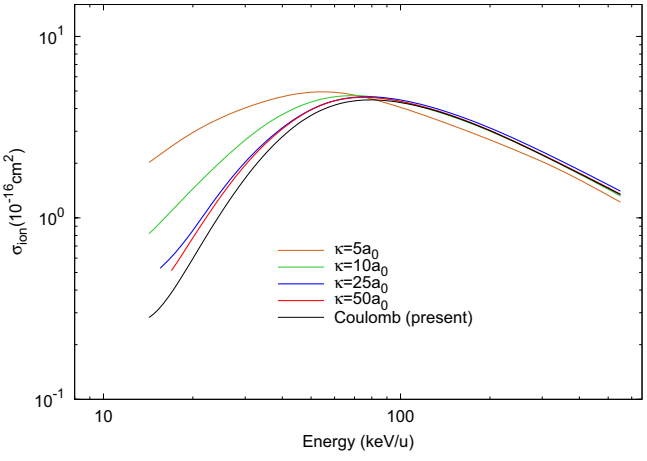

Fig. 9. Ionization cross sections for plasmas with screening lengths $\kappa = 5, 10, 25, 50a_0$ and for the pure Coulomb interaction.

4.3 Ionization

Since in the expansion basis (5) we have included 117 continuum pseudostates centered on the target H, the transitions to these states in the course of the collision would describe the ionization process. The total ionization cross section is given by equation (7c), where the summation runs over all continuum pseudostates. As discussed in the Introduction, in the screened potential (1) for any finite value of the scaled screening length κ_0 the number of bound states is finite. From Table 1 it follows that for a given value κ_0 bound are the nl-states with critical screening lengths satisfying the relation $\kappa^c_{nl} < \kappa_0$, while all the states with $\kappa^c_{nl} > \kappa_0$ lie in the continuum i.e. become continuum pseudostates. Thus, for $\kappa_0 = 30a_0$ bound in the potential (2) are only the states with $n \leq 4$ (cf. Tab. 1) and all the $5l$, $6l$ and $7s$ included in our discrete Coulomb basis on H (see Sect. 3) become continuum pseudostates. When calculating the ionization cross section for a given κ_0, the population of the continuum pseudostates, that are generated from entering the discrete states with $\kappa^c_{nl} > \kappa_0$ into the continuum, have also to be included in the sum of equation (7c).

In Figure 9 we show the ionization cross sections for plasmas with screening lengths $\kappa = 5, 10, 25, 50a_0$ in the energy range ∼15–500 keV/u. For the above values of κ the only bound states in the potential (2) are $1s$, (for $5a_0$), $n \leq 2$ (for $10a_0$), $n \leq 3 + 4s$ (for $25a_0$), and $n \leq 5$ (for $50a_0$). In the same figure we also show the cross section for the pure Coulomb interaction. We note that the ionization cross section of reference [22] for the pure Coulomb case coincides with the result of our calculations, but is not shown in Figure 9 to preserve the clarity of the figure in the high energy part.

In Figure 9 two different dependences of the ionization cross section on the screening length are observed. For energies above ∼70–80 keV/u, where the cross section maxima appear, the screened cross sections rapidly tend towards the unscreened cross section when the screening

length increases (i.e. they decrease with decreasing κ). In contrast to this, for energies below ∼70–80 keV/u, the ionization cross section increases with decreasing κ. This increase can be related to the fact that with decreasing κ increasingly more bound states in the expansion basis centered on the target H enter in the continuum. This increases the density of continuum pseudostates and, consequently, the ionization cross section. It is to be noted in Figure 9 that with decreasing κ also the cross section maximum shifts to lower energies. The relatively weak dependence of the cross section on κ at high energies is result of the fact that the energies of continuum pseudostates, generated by entering of bound states into the continuum when κ decreases, are small but also due to the fact that at high collision energies the atomic electron is ejected predominantly to high-energy continuum states.

5 Conclusions

In the present work, we have studied the excitation, electron capture and ionization processes in collisions of He^{2+} ions with hydrogen atoms in a dense quantum plasma. The interaction between charged particles in such a plasma is represented by the Debye-Hückel-cosine (DHC) screened potential. The collision dynamics of considered processes is described by the two-center atomic orbital close coupling method with an expansion basis containing 35 bound states centered on the projectile and 57 bound plus 117 continuum pseudostates centered on the target. The investigations of plasma screening effects on the considered processes reveal significant changes in their cross sections with respect to those in the plasma-free case, when the interaction is purely Coulombic. These effects are particularly strong when the screening is strong (small screening lengths) and for the smaller collision energies (long collision times). The property of DHC screened potential to support a finite number of bound states for any finite value κ_0 of its screening length (implying that for $\kappa > \kappa_0$ higher states lie in the continuum) has a dramatic effect on the low-energy ionization cross sections (dramatic increase with decreasing of κ and the energy). For the processes taking place within the discrete spectrum (excitation and electron capture, this property of DHC potential limits the collision dynamics to a limited number of bound states, as opposed to the theoretically infinite number of bound states in the case of pure Coulomb potential.

For the cases of excitation to $2s, 2p$ states and electron capture to $1s, 2s$ and $2p$ states we have compared the cross sections in the $He^{2+} + H$ and $H^+ + H$ collision systems for the same screening length $\kappa = 10a_0$ to elucidate the difference in the collision dynamics in a quantum plasma in a homonuclear and heteronuclear collision system. Significant differences in the energy behavior and magnitudes of electron cross sections are observed, arising from the existence (or absence) of nuclear symmetry in the collision system and from the difference of number of bound states on the projectile available for electron capture. The observed differences in the excitation cross sections are only due to the strength parameter Z of the potential (1).

Author contribution statement

The authors contributed equally to the paper.

References

1. P. Debye, E. Hückel, Phys. Z. **24**, 185 (1923)
2. R.K. Janev, S.B. Zhang, J.G. Wang, Matter Radiat. Extreme **1**, 237 (2016)
3. P.K. Shukla, B. Eliasson, Phys. Lett. A **372**, 2897 (2008)
4. L.G. Stanton, M.S. Murillo, Phys. Rev. E **91**, 033104 (2015)
5. G.P. Zhao, L. Liu, J.G. Wand, R.K. Janev, Phys. Plasmas **24**, 103504 (2017)
6. D. Jakimovski, N. Markovska, R.K. Janev, J. Phys. B: At. Mol. Phys. **49**, 205701 (2016)
7. A. Ghoshal, Y.K. Ho, J. Phys. B **42**, 175006 (2009)
8. I. Nasser, M.S. Abdelmonem, A. Abdel-Hady, Phys. Scr. **84**, 045001 (2011)
9. A. Ghoshal, Y.K. Ho, Phys. Scr. **83**, 065301 (2011)
10. A. Bhattacharya, Z.M. Kamali, A. Ghoshal, K. Ratnavelu, Phys. Plasmas **20**, 083514 (2013)
11. S. Nayek, A. Ghoshal, Phys. Scr. **85**, 035301 (2012)
12. N.F. Lai, Y.C. Lin, C.Y. Lin, Y.K. Ho, Chin. J. Phys. **51**, 73 (2013)
13. C.Y. Lin, Y.K. Ho, Comput. Phys. Commun. **182**, 125 (2011)
14. L.-Y. Zhang, X. Qi, X.-Y. Zhao, D.-Y. Meng, G.-Q. Xiao, W.-S. Duan, L. Yang, Phys. Plasmas **20**, 113301 (2013)
15. L.-Y. Zhang, X.-Y. Zhao, J.-F. Wan, G.-Q. Xiao, W.-S. Duan, X. Qi, L. Yang, Phys. Plasmas **21**, 093302 (2014)
16. Y.Y. Qi, J.G. Wang, R.K. Janev, Phys. Plasmas **23**, 073302 (2016)
17. Y.Y. Qi, J.G. Wang, R.K. Janev, Phys. Plasmas **24**, 062110 (2017)
18. B.H. Bransden, M.R.C. McDowell, *Charge Exchange and the Theory of Ion-Atom Collisions* (Clarendon Press, Oxford, 1992)
19. L.D. Landau, E.M. Lifshitz, *Quantum Mechanics: Non-Relativistic Theory* (Pergamon, London, 1958)
20. W. Fritsch, C.D. Lin, Phys. Rep. **202**, 1 (1991)
21. C.M. Reeves, J. Chem. Phys. **39**, 1 (1963)
22. J. Kuang, C.D. Lin, J. Phys. B **30**, 101 (1997)